BiVO₄ as a Visible-Light Photocatalyst Prepared by Ultrasonic Spray Pyrolysis

Scott S. Dunkle, Richard J. Helmich, and Kenneth S. Suslick*

School of Chemical Sciences, University of Illinois at Urbana−Champaign, 600 S. Mathews Avenue, Urbana, Illinois 61801

BiVO₄ powders with unique particle architectures have been synthesized using ultrasonic spray pyrolysis (USP). Gases created from the evaporation of solvent and the decomposition of precursor materials shape the morphology of the particles as the solids are formed in the heated aerosol. The BiVO₄ powder was tested as oxygen evolving photocatalysts by monitoring the kinetics of O₂ formation from a AgNO₃ solution irradiated with $\lambda > 400$ nm light. USP prepared BiVO₄ was found to have significantly superior photocatalytic activity compared to commercial BiVO₄ and WO₃, likely due to differences in particle morphology.

Introduction

Fossil fuels have supplied a majority of the world's energy requirements for hundreds of years, but with rising energy demands and dwindling fuel-stocks, dramatic new emphasis is now being placed on solar energy conversion technologies.[1−4] Since the experiments of Fujishima and Honda that demonstrated the electrophotolysis of water using a TiO₂ catalyst,[5] a flurry of attention has been directed toward developing photocatalysts for water splitting. Metal oxides are a popular choice for water splitting applications,[4,6−9] but their band gaps are generally wide, which makes photocatalysis possible only with UV radiation. Since a substantial portion of the sun's radiation lies within the visible spectrum, finding visible-light active photocatalysts is of particular importance.[10−12]

BiVO₄ is well-known for its ferroelastic properties[13] and its use as a nontoxic, bright yellow pigment[14,15] and has received some attention as a visible-light active photocatalyst.[16−18] The oxide has been synthesized by various means, including traditional solid state,[19−21] hydrothermal,[22,23] sonochemical,[24] and aqueous/coprecipitation.[16,25,26] With a bandgap of 2.4 eV, BiVO₄ absorbs well into the visible spectrum and has shown significant visible-light activity for O₂ evolution from AgNO₃ solutions, which act as the oxidizing agent.[16−18] The monoclinic sheelite polymorph of BiVO₄ is known to possess the highest photocatalytic activity,[16] however two other forms of the material do exist (tetragonal zircon and tetragonal sheelite).[27] Previous photocatalytic experiments conducted in methanol solutions (which provide hole-scavenging) have shown that BiVO₄ is unable to evolve hydrogen,[17] which implies that the conduction band of the semiconductor lies more positive than the H⁺/H₂ redox potential. Despite this shortcoming, BiVO₄ remains an interesting oxygen evolving photocatalyst that can be applied to Z-scheme systems with a separate H₂ evolving photocatalyst to complete the overall water splitting reaction.[28,29]

Ultrasonic spray pyrolysis (USP)[30−32] is a powerful synthetic method for the production of a diverse range of micro and nanostructured products that include metal chalcogenide quantum dots[33] and catalysts,[34,35] metal oxides,[36−41] and novel morphologies of high surface area carbons.[42−45] With USP, ultrasound is applied to a precursor solution in order to create an aerosol that is then swept by a carrier gas through a furnace. Upon heating, the precursor solvent evaporates and precursors decompose resulting in a product with a generally spherical shape. With low volatility precursors, each droplet in the aerosol can be thought of as an individual subpicoliter reactor (subμm diameter) that guides particle morphology. In addition, gases created from the evaporation of solvent and the decomposition of precursor materials shape the nanostructure the solids formed in the heated aerosol.

Herein, we describe a facile one-step process using USP without the use of preformed templates to generate micrometer sized BiVO₄ particles with unique architectures. In addition, as is the case for all USP methods, the process is continuous and easily scalable. Lastly, the BiVO₄ powders were tested for visible-light photocatalytic activity toward O₂ evolution from AgNO₃ solution, and the USP prepared BiVO₄ was found to have significantly superior photocatalytic activity compared to commercial BiVO₄ and WO₃.

Experimental Section

USP Apparatus. The USP experimental setup has been described elsewhere in more detail.[35,40,41] In brief, a piezoceramic transducer operating at 1.65 MHz was used to nebulize a precursor solution into a micrometer-sized mist. The mist was then carried by air flow (∼1 standard liter/min) into a furnace at a temperature of 700 °C. The products were collected in water-filled bubblers at the furnace outlet. A schematic of this setup is shown in the Supporting Information (SI Figure S1).

Materials and Precursor Solution Preparation. Bismuth nitrate pentahydrate (Bi(NO₃)₃·5H₂O, 99.99+% purity) was obtained from Sigma-Aldrich, whereas ammonium metavanadate (NH₄VO₃, 99% purity) was obtained from Strem. All materials were used as received. In a typical precursor solution preparation, a 1:1 mol ratio of Bi(NO₃)₃·5H₂O and NH₄VO₃ were dissolved in a ∼3 M solution of nitric acid. Precursors were added to obtain a final concentration of 0.2 M. Stirring is recommended to ensure a homogeneous solution mixture.

---

* To whom correspondence should be addressed. E-mail: ksuslick@illinois.edu.

Letters

J. Phys. Chem. C, Vol. 113, No. 28, 2009 **11981**

Product Isolation. USP products were isolated from the aqueous bubbler suspensions by centrifugation and washed a minimum of three times with purified water and then once with absolute ethanol. The powder was then dried under vacuum at room temperature for ~12 h prior to characterization.

Characterization of BiVO$_4$ Powders. All powder X-ray diffraction (XRD) measurements were conducted with a Rigaku D-MAX diffractometer using Cu Kα radiation and operated at 45 kV and 20 mA with a scan rate of 1°/min and step size of 0.02°. To observe particle morphology, scanning electron micrographs (SEM) were taken using a JEOL 7000F operating at 15 kV while transition electron microscopy (TEM) was conducted using a JEOL 2100 Cryo operating at 200 kV. Diffuse reflectance UV−vis measurements were taken using a Hitachi 3300 double monochromator UV−vis spectrophotometer. Surface area measurements taken with a Nova 2200e Surface Area and Pore Analyzer (Quantachrome Instruments) at liquid nitrogen temperature (−196 °C), whereas surface areas were obtained using the BET method.

Photocatalytic Testing. Photocatalytic reactions were carried out using a standard inner-radiation reaction vessel with a water-jacketed Pyrex immersion well connected to a closed gas handling system. Oxygen evolution was detected with an online gas chromatograph (GC) equipped with a thermal conductivity detector (Agilent 6890 GC, G1532−60720 TCD). All reactions were run in 500 mL of a 50 mM AgNO$_3$ solution and were irradiated with a 450 W medium-pressure Hg lamp. Flowing within the water-jacket of the immersion well was a 1 M solution of NaNO$_2$ used to block wavelengths of light shorter than 400 nm. A total of 500 mg of catalyst was used in each reaction and was kept suspended with magnetic stirring. The quantum efficiency of O$_2$ production of the BiVO$_4$ generated by USP was performed using a 300 W Xe CERMAX lamp with 50 mg of catalyst and 50 mL of AgNO$_3$ solution (which is optically dense) and was calculated employing the equation

$$Q.E.(\%) = \frac{\text{number of evolved O}_2 \text{ molecules} \times 4}{\text{number of incident photons}} \times 100 \quad (1)$$

where the number of incident photons was measured at various wavelengths using narrow band-pass filters (half width = 10 nm) and chemical actinometry using potassium ferrioxalate solutions.[46] All photons were assumed to be absorbed by the photocatalyst (i.e., light scattering is ignored so the QE is therefore a lower limit).

Results and Discussion

Particle Morphology. BiVO$_4$ powder prepared by USP contains particles with unique architectures. SEM and TEM micrographs (Figure 1) clearly show mostly hollow shells (Figure 1E) or fractions of hollow shells (while retaining the generally spherical shape typical of USP synthesized products). In addition, many of these shell structures contain macropores (Figure 1C) or "blow-outs" (Figure 1A). It was also found that some of the hollow shells even contain smaller spheres sitting inside, creating a "ball-in-ball" type structure (Figure 1, panels B and F). The development of these types of intriguing particle morphologies lead to considerably higher surface areas than for materials made using traditional solid state reaction techniques. Nitrogen adsorption studies show that BiVO$_4$ created using USP has a surface area of 3.2 m^2/g while a commercially available BiVO$_4$ powder (Alfa Aesar) has a surface area of only 0.45 m^2/g.
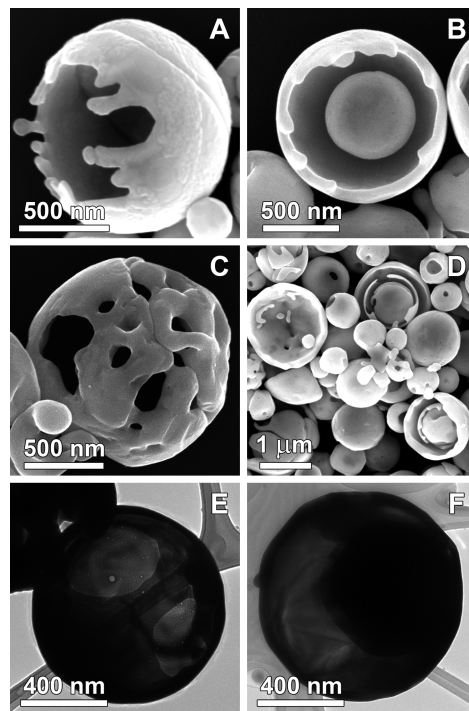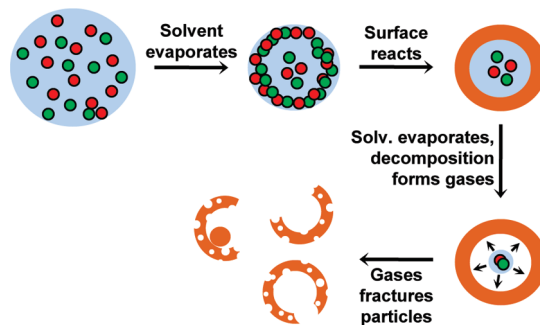

Figure 1. (A−D) SEM and (E and F) TEM micrographs illustrating typical particle morphologies obtained during USP synthesis of BiVO$_4$.

SCHEME 1: Mechanism of Particle Formation for BiVO$_4$ Powder Prepared by USP

The mechanism behind the BiVO$_4$ particle formation is of particular interest considering that the hollow shell morphology is obtained without the use of templating. Previous work performed by Okuyama and co-workers[37] studied the synthesis of ZrO$_2$ by spray pyrolysis in order to understand the conditions necessary for hollow particle formation. Their studies showed that at high furnace temperature (500−700 °C), hollow and often broken shells would form due to the quick evaporation of the solvent, producing a high precursor concentration at the surface of the droplet. Okuyama and co-workers propose a product shell can thereby be created from the supersaturation, precipitation and decomposition at the droplet surface. The center of the particle is then filled with remaining precursor and solvent, which evaporates or decomposes, exerting pressure from the inside of the particle, creating hollow particles or broken shells.

We believe the formation of BiVO$_4$ particles occurs by a similar mechanism (Scheme 1). The thermal decomposition of Bi(NO$_3$)$_3$ and NH$_4$VO$_3$ results in the evolution of NO$_x$, NH$_3$, and H$_2$O gas[47,48] which, if formed inside a shell of BiVO$_4$, could form the blow-outs, pores, and broken shells seen in the final product. In addition, the ball-in-ball type structure is likely the result of remnant precursor decomposition inside the already formed outer shell.
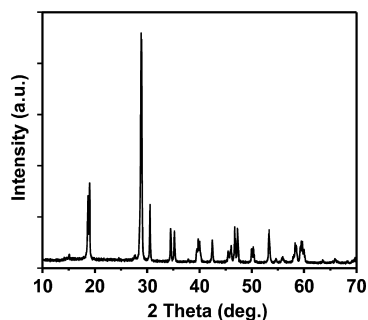
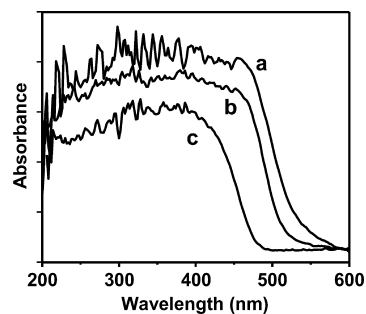**Figure 2.** Powder X-ray diffraction pattern of USP prepared BiVO₄.

Figure 3. Diffuse reflectance spectra obtained for (a) commercially available BiVO₄, (b) BiVO₄ prepared by USP, and (c) commercially available WO₃.

Figure 4. (A) Plot indicating the amount of oxygen evolved over time from BiVO₄ prepared by USP, and commercially available BiVO₄ and WO₃ in a 50 mM AgNO₃ solution with $\lambda > 400$ nm irradiation and (B) a comparison of maximum and average photocatalytic activities of each of the photocatalysts (averages for first 5 h of activity).

There is a notable difference, however, between the prior work with ZrO_2 and our observations on $BiVO_4$: ZrO_2 did not show signs of pores or blow-outs, only broken shells. ZrO_2 has a melting point of approximately 2700 °C, whereas the melting point of $BiVO_4$ is much less, ∼940 °C. During synthesis at 700 °C, $BiVO_4$ is most likely in a softened state, leading to the formation of pores (i.e., localized blow-outs, instead of complete fragmentation), finger-like appendages (where gases have left the inner core), and smoothing of the outer edges of all the particles. At the same temperature, ZrO_2 is rigid and simply fractures after sufficient build-up of internal gas pressure.

Powder X-ray Diffraction. Powder X-ray diffraction was performed on $BiVO_4$ prepared by USP to determine the phase of the synthesized product. The low temperature phase of $BiVO_4$ is tetragonal zircon and converts irreversibly at 397−497 °C to the high temperature monoclinic phase.[21] Given the reaction conditions (700 °C), monoclinic is the expected phase of the material. As can be seen in Figure 2, the XRD pattern shows a pair of peaks at $2\theta = 18.68°$ and 18.98°, which is representative of the monoclinic sheelite phase. No other phases are seen in the diffraction pattern, and the narrow line widths indicate a high degree of crystallinity (crystallite size >150 nm).

Photocatalytic Activity. Since previous work has shown that $BiVO_4$ is an active material for O_2 evolution from $AgNO_3$ solution under visible light irradiation, the photocatalytic activity of $BiVO_4$ prepared by USP was tested and compared to commercially available $BiVO_4$ (Alfa Aesar) and WO_3 (Sigma-Aldrich). Figure 3 shows diffuse reflectance spectra taken for each of the materials. Each of the samples absorb well into the visible spectrum, suggesting each should be active for visible light photocatalysis. Based on extrapolations of the straight portions of the absorption edge, it can be estimated that $BiVO_4$ prepared by USP has a band gap of 2.4 eV. Commercial $BiVO_4$ has a similar band gap of 2.3 eV, and the band gap of commercial WO_3 is about 2.6 eV. $BiVO_4$ is unique in that its valence band is comprised of a coupling between the Bi 6s and
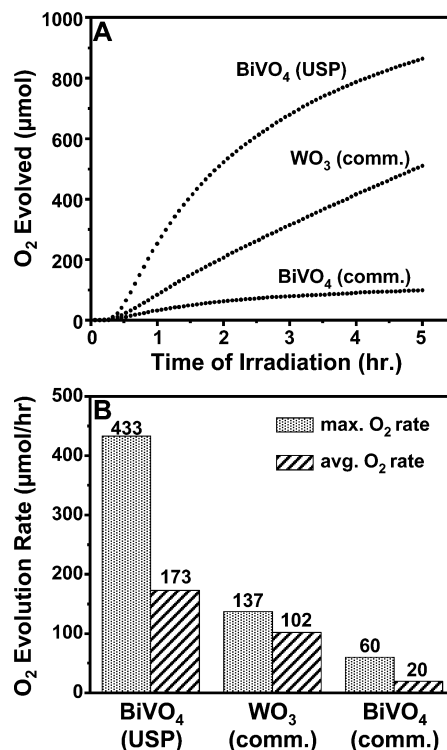
O 2p orbitals which causes a destabilization and forces the valence band upward.[49−51] Conversely, the conduction band involves a coupling between the V 3d, O 2p, and Bi 6p, which lowers the band. This results in a direct band gap semiconductor[51] with a smaller band gap than most oxides and enhanced visible light absorption, leading to its bright yellow color. In addition, the coupling of the Bi 6s and O 2p in the valence band allow for improved hole mobility,[51] which is beneficial for photocatalytic oxidation reactions.

Figure 4A shows the results of photocatalytic experiments with the above-mentioned oxides in $AgNO_3$ solution irradiated >400 nm. $BiVO_4$ synthesized by USP is considerably more active for O_2 evolution than either commercially available $BiVO_4$ or WO_3. The observed decline in activity over extended periods of time can be attributed to the buildup of Ag metal on the surface of the photocatalysts from photoreduction. A summary of the photocatalytic activity of each of the materials can be found in Figure 4B. Maximum O_2 evolution rates for $BiVO_4$ prepared by USP and commercial $BiVO_4$ and WO_3 were 433, 60, and 137 μmol/h, respectively. Based on this information, the synthesis of $BiVO_4$ by USP results in a photocatalyst that is roughly seven times more active than commercially available $BiVO_4$ and about three times more active than commercial WO_3, which is the most commonly used photocatalyst for O_2 generation.[4] Actinometry measurements indicate the USP product has a quantum efficiency of 2.58% at $\lambda = 400$ nm for oxygen evolution.

The increased O_2 evolution observed for USP generated $BiVO_4$ appears to be a function of higher surface area due to the hollow particle morphology, rather than crystallinity or absorption edge. The improved activity is not due to the extent of crystallinity, since all of the catalysts are highly crystalline, as shown by the XRD (cf. Figure 2 and SI Figure S2).

Letters

J. Phys. Chem. C, Vol. 113, No. 28, 2009 **11983**

Furthermore, there is no drastic difference between the absorption at 400 nm of the $BiVO_4$ catalysts (Figure 3), yet there is a large difference in photocatalytic activity. In addition, WO_3 absorbs less visible light than $BiVO_4$, but its activity is higher than that of commercial $BiVO_4$. This is likely due to the O 2p valence band of WO_3 lying at a more positive potential[52] than the mixed Bi 6s O 2p valence band of $BiVO_4$. This gives WO_3 an increased driving force for the oxidation of water compared to $BiVO_4$. While this is enough for the WO_3 to outperform the activity of commercial $BiVO_4$, it is not enough to outperform the USP prepared product.

Both commercial materials have a similar particle morphology (cf. SEM micrographs in SI Figure S3) which are large (∼2 μm) particles due to traditional solid state synthesis techniques. In stark contrast, the USP synthesized product is composed of thin shells. Previous work with $BiVO_4$ nanoparticles has shown that particles with larger dimension have decreased photocatalytic activity toward oxygen evolution associated with the distance electron−hole pairs must travel through the material.[53] When electron−hole pairs are generated in an irradiated solid, the charge carriers must move through the material and reach the surface in order to perform the desired redox reactions. If the pair is generated deep inside a large particle, the probability of the electron and hole recombining before they reach the surface is increased substantially compared to a nanostructured material. In a nanostructured material, the electron and hole inherently are already very near the surface, discouraging recombination. This phenomenon would result in the increased photocatalytic activity from the USP generated $BiVO_4$ compared to conventional $BiVO_4$ powders.

Conclusions

USP provides a one-step, continuous, and scalable process for the template-free production of nanostructured $BiVO_4$ with particles ranging from thin hollow and porous shells to ball-in-ball type structures. Particle morphologies are likely due to the initial formation of an oxide shell on the aerosol droplet surface and subsequent ballooning from the evaporation of solvent and development of precursor decomposition gases inside the shell. Photocatalytic testing reveals $BiVO_4$ synthesized by USP is significantly more active for O_2 evolution under visible-light irradiation in $AgNO_3$ solution than commercial $BiVO_4$ and WO_3 powders. The increased photocatalytic activity is likely due to the short distances electron−hole pairs must move to reach the surface of the shells in the USP product.

Supporting Information Available: Schematic of the USP setup and additional commercial materials characterization (XRD, SEM, quantum efficiencies). This material is available free of charge via the Internet at http://pubs.acs.org.

References and Notes

(1) Gratzel, M. *Inorg. Chem.* **2005**, *44*, 6841.
(2) Kamat, P. V. *J. Phys. Chem. C* **2007**, *111*, 2834.
(3) Lewis, N. S.; Nocera, D. G. *Proc. Natl. Acad. Sci. U.S.A.* **2006**, *103*, 15729.
(4) Osterloh, F. E. *Chem. Mater.* **2008**, *20*, 35.
(5) Fujishima, A.; Honda, K. *Nature* **1972**, *238*, 37.
(6) Kato, H.; Kudo, A. *Chem. Phys. Lett.* **1998**, *295*, 487.
(7) Kudo, A. *Int. J. Hydrogen Energy* **2006**, *31*, 197.
(8) Sayama, K.; Arakawa, H. *J. Photochem. Photobiol. A* **1994**, *77*, 243.
(9) Takata, T.; Tanaka, A.; Hara, M.; Kondo, J. N.; Domen, K. *Catal. Today* **1998**, *44*, 17.
(10) Maeda, K.; Domen, K. *J. Phys. Chem. C* **2007**, *111*, 7851.
(11) Maeda, K.; Teramura, K.; Saito, N.; Inoue, Y.; Kobayashi, H.; Domen, K. *Pure Appl. Chem.* **2006**, *78*, 2267.
(12) Yamasita, D.; Takata, T.; Hara, M.; Kondo, J. N.; Domen, K. *Solid State Ionics* **2004**, *172*, 591.
(13) Bhattacharya, A. K.; Mallick, K. K.; Hartridge, A. *Mater. Lett.* **1997**, *30*, 7.
(14) Piltingsrud, D. H. U.S. Patent 4,115,141,1978.
(15) Hess, R. W. U.S. Patent 4,115,142, 1978.
(16) Kudo, A.; Omori, K.; Kato, H. *J. Am. Chem. Soc.* **1999**, *121*, 11459.
(17) Kudo, A.; Ueda, K.; Kato, H.; Mikami, I. *Catal. Lett.* **1998**, *53*, 229.
(18) Tokunaga, S.; Kato, H.; Kudo, A. *Chem. Mater.* **2001**, *13*, 4624.
(19) Roth, R. S.; Waring, J. L. *Am. Mineral.* **1963**, *48*, 1348.
(20) Sleight, A. W.; Chen, H. y.; Ferretti, A.; Cox, D. E. *Mater. Res. Bull.* **1979**, *14*, 1571.
(21) Lim, A. R.; Choh, S. H.; Jang, M. S. *J. Phys.: Condens. Matter* **1995**, *7*, 7309.
(22) Yu, J.; Kudo, A. *Adv. Funct. Mater.* **2006**, *16*, 2163.
(23) Zhang, L.; Chen, D.; Jiao, X. *J. Phys. Chem. B* **2006**, *110*, 2668.
(24) Zhou, L.; Wang, W.; Liu, S.; Zhang, L.; Xu, H.; Zhu, W. *J. Mol. Catal. A: Chem.* **2006**, *252*, 120.
(25) Yu, J.; Zhang, Y.; Kudo, A. *J. Solid State Chem.* **2009**, *182*, 223.
(26) Zhou, L.; Wang, W.; Zhang, L.; Xu, H.; Zhu, W. *J. Phys. Chem. C* **2007**, *111*, 13659.
(27) Bierlein, J. D.; Sleight, A. W. *Solid State Commun.* **1975**, *16*, 69.
(28) Abe, R.; Sayama, K.; Sugihara, H. *J. Phys. Chem. B* **2005**, *109*, 16052.
(29) Sasaki, Y.; Iwase, A.; Kato, H.; Kudo, A. *J. Catal.* **2008**, *259*, 133.
(30) Kodas, T. T.; Hampden-Smith, M. *Aerosol Processing of Materials*; Wiley: New York, 1999.
(31) Okuyama, K.; Abdullah, M.; Lenggoro, I. W.; Iskandar, F. *Advanced Powder Technology* **2006**, *17*, 587.
(32) Swihart, M. T. *Curr. Opin. Colloid Interface Sci.* **2003**, *8*, 127.
(33) Didenko, Y. T.; Suslick, K. S. *J. Am. Chem. Soc.* **2005**, *127*, 12196.
(34) Bang, J. H.; Helmich, R. J.; Suslick, K. S. *Adv. Mater.* **2008**, *20*, 2599.
(35) Skrabalak, S. E.; Suslick, K. S. *J. Am. Chem. Soc.* **2005**, *127*, 9990.
(36) Hampsey, J. E.; Arsenault, S.; Hu, Q.; Lu, Y. *Chem. Mater.* **2005**, *17*, 2475.
(37) Widiyastuti, W.; Wang, W.-N.; Lenggoro, I. W.; Iskandar, F.; Okuyama, K. *J. Mater. Res.* **2007**, *22*, 1888.
(38) Jiang, X.; Brinker, C. J. *J. Am. Chem. Soc.* **2006**, *128*, 4512.
(39) Prakash, A.; McCormick, A. V.; Zachariah, M. R. *Nano Lett.* **2005**, *5*, 1357.
(40) Suh, W. H.; Jang, A. R.; Suh, Y.-H.; Suslick, K. S. *Adv. Mater.* **2006**, *18*, 1832.
(41) Suh, W. H.; Suslick, K. S. *J. Am. Chem. Soc.* **2005**, *127*, 12007.
(42) Bang, J. H.; Han, K.; Skrabalak, S. E.; Kim, H.; Suslick, K. S. *J. Phys. Chem. C* **2007**, *111*, 10959.
(43) Hampsey, J. E.; Hu, Q.; Rice, L.; Pang, J.; Wu, Z.; Lu, Y. *Chem. Commun.* **2005**, 3606.
(44) Skrabalak, S. E.; Suslick, K. S. *J. Am. Chem. Soc.* **2006**, *128*, 12642.
(45) Zheng, T.; Zhan, J.; Pang, J.; Tan, G. S.; He, J.; McPherson, G. L.; Lu, Y.; John, V. T. *Adv. Mater.* **2006**, *18*, 2735.
(46) Calvert, J. G.; Pitts, J. N., Jr. *Photochemistry*; Wiley: New York, 1966.
(47) Coppa, N. V.; Hults, W. L.; Smith, J. L.; Brynestad, J. *J. Mater. Res.* **1994**, *9*, 2510.
(48) Taniguchi, M.; Ingraham, T. R. *Can. J. Chem.* **1964**, *42*, 2467.
(49) Sayama, K.; Nomura, A.; Arai, T.; Sugita, T.; Abe, R.; Yanagida, M.; Oi, T.; Iwasaki, Y.; Abe, Y.; Sugihara, H. *J. Phys. Chem. B* **2006**, *110*, 11352.
(50) Stoltzfus, M. W.; Woodward, P. M.; Seshadri, R.; Klepeis, J.-H.; Bursten, B. *Inorg. Chem.* **2007**, *46*, 3839.
(51) Walsh, A.; Yan, Y.; Huda, M. N.; Al-Jassim, M. M.; Wei, S.-H. *Chem. Mater.* **2009**, *21*, 547.
(52) Bamwenda, G. R.; Arakawa, H. *Appl. Catal., A* **2001**, *210*, 181.
(53) Ke, D.; Peng, T.; Ma, L.; Cai, P.; Jiang, P. *Appl. Catal. A* **2008**, *350*, 111.